World Academy of Science, Engineering and Technology
International Journal of Civil and Environmental Engineering
Vol:6, No:8, 2012

The Effect of Intermediate Stiffeners on Steel Reinforced Concrete Beams Behaviors

Teguh Sudibyo, Cheng-Cheng Chen

Abstract**—**Eight steel reinforced concrete beams (SRC), were fabricated and tested under earthquake type cyclic loading. The effectiveness of intermediate stiffeners, such as mid-span stiffener and plastic hinge zone stiffeners, in enhancing composite action and ductility of SRC beams was investigated. The effectiveness of strengthened beam-to-column (SBC) and weakened beam-to-column (WBC) connections in enhancing beam ductility was also studied. It was found that: (1) All the specimens possessed fairly high flexural ductility and were found adequate for structures in high seismic zones. (2) WBC connections induced stress concentration which caused extra damage to concrete near the flange tapering zone. This extra damage inhibited the flexural strength development and the ductility of the specimens with WBC connections to some extent. (3) Specimens with SBC connections demonstrated higher flexural strength and ductility compared to specimens with WBC connections. (4) The intermediate stiffeners, especially combination of plastic hinge zone stiffener and mid span stiffeners, have an obvious effect in enhancing the ductility of the beams with SBC connection.

Keywords**—**Composite beam, concrete encased steel beam, steel reinforced concrete, stiffeners.

I. Introduction

STEEL reinforced concrete (SRC) is typically comprised of steel structural members characterized by a cross sectional shape and accompanied by longitudinal and transverse steel bars for further reinforcement. This type of composite beam is used in seismic resistant moment frames and offer several advantages, including higher fire resistance, higher stiffness, and higher flexural strength, over plain steel beams.

Chen [1] completed a series of large-scale fully encased steel beam loading tests. The beams were simply supported and were loaded monotonically by 2-point loads, as shown in Fig. 1(a). Four of the tested beams, listed in Table I, were selected and are discussed in this study. There are three possible stress transfer mechanisms by which interface stresses can be transferred between the steel shapes and the concrete; they are: natural bonds, shear connectors and stiffeners. The test beams are arranged in a way that allows the effectiveness of the stress transfer mechanism to be examined. Table I shows the stress transfer mechanism combination that is used for each beam, and Fig. 1 shows the details of the test beams. Fig. 2 shows the measured moment vs. curvature relationship of the test beams.

T. Sudibyo is Ph.D. student in National Taiwan University of Science and Technology, ROC and lecturer in the Department of Civil Engineering, Universitas Gadjah Mada, Indonesia (e-mail: D9505805@mail.ntust.edu.tw).

C.C. Chen is the professor in the Department of Construction Engineering, National Taiwan University of Science and Engineering, Taipei, ROC. (e-mail: c3@mail.ntust.edu.tw).

It was observed that slip occurred between the steel shape and the concrete at the beam ends for S1-NN. Among the three beams shown in Fig. 2(a), it was found that in terms of flexural strength and ductility, S1 and S1-NB demonstrate similar behavior, which is far superior to the behavior of S1-NN. This implies that end stiffeners have a more significant positive influence on the beam behavior than natural bonds. It can be observed from Fig. 2(b) that when the end stiffeners were used, the shear studs did not have an extra positive influence on the beam strength and ductility. In the case of simply supported beams, end stiffeners seemed to constrain the concrete and activate the composite action of the beam.

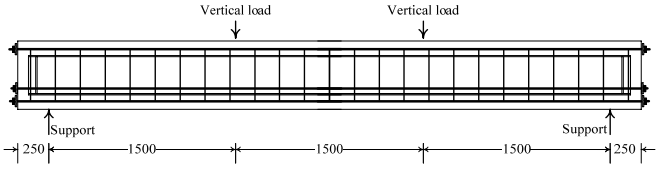

(a) SRC beam

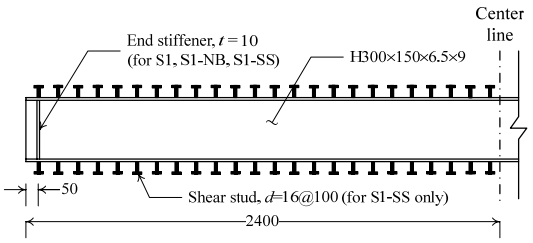

(b) H section

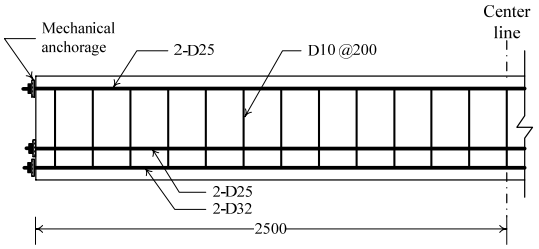

(c) RC section

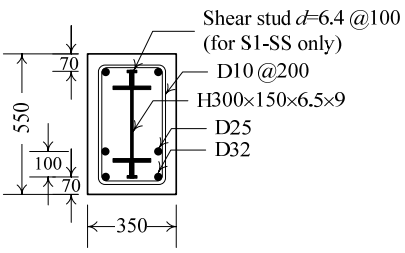

(d) SRC cross section

TABLE I
SPECIMENS USED IN CHEN [1]

Specimen designation	Stress transfer type		
	End stiffener	Natural bond	Shear stud
S1	√	√	×
S1-NB	√	×	×
S1-NN	×	×	×
S1-SS	√	√	√

Fig. 1 Chen's SRC specimen [1] (unit: mm)

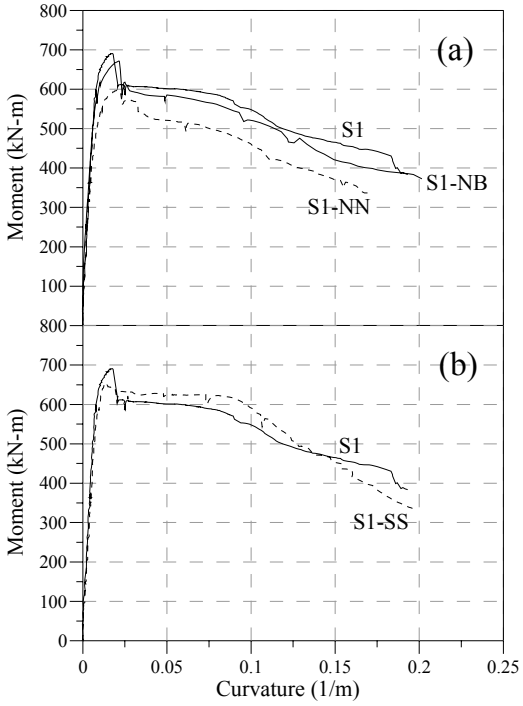

Fig. 2 Chen's test results [1]

When a beam forms part of a moment resisting frame (MRF), constraint to the concrete can be provided by columns connected to the beam and suppresses the slip between concrete and steel shape surface. This column constraint should have positive effect on developing beam's composite action. However, when the distance between beam ends, or columns, is too far, the effect of the column constraint may be reduced. In this case, intermediate stiffeners may provide extra constraint and provide more concrete confinement which may enhance the ductility of the beam. For the beam shown in Fig. 3 subjected to earthquake type loading, a stiffener at the mid-span, where bending moment changes direction, may be helpful. In addition, a stiffener near the plastic hinge zone, where the requirement for composite action is the highest in the beam span, should be advantageous.

In steel structures, it is common practice to move the plastic hinge away from the column surface to prevent premature fractures of the welds connecting the beam flange and the column flange. SBC and WBC connections have been suggested to solve this problem [2]-[6]. SRC beam has the same concern as steel beam does. And, it is of interest to the authors how SRC beams perform when SBC or WBC is employed.

In this study, a total of 8 SRC beam specimens were fabricated and tested under earthquake type loading. The effectiveness of column constraint and intermediate stiffeners was investigated. In addition, the suitability of SBC and WBC to SRC beams is assessed.

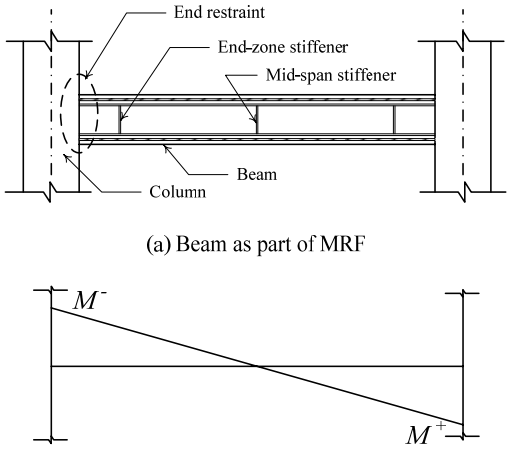

Fig. 3 Beam under earthquake type loading

II. EXPERIMENTAL PROGRAM

A. Test Specimens

Table II shows the designations of the 8 specimens tested. Each test specimen was mounted to a pair of columns with much higher relative stiffness and strength using end-plate connections, as shown in Fig. 4. The end-plate connection was designed such that the deformation of the connection was negligible. All the specimens have a clear span length (L_b) of 1200 mm. The bottom end of each column was connected to a strong floor through a hinge. The distance from the column hinge to the center of the beam (L_c) was 1200 mm.

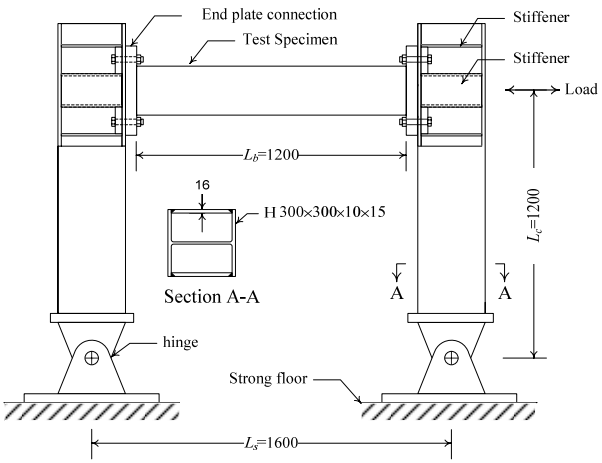

Fig. 4 The test scheme for beam specimens (unit: mm)

Fig. 5 shows the geometry and dimensions of the cross-section used. The section has a rectangular cross-section of 145 mm × 220 mm.

TABLE II
SPECIMENS AND THE TEST RESULTS

Specimen	P^{+}_{peak} (kN)	α^{+}_{peak} (%)	P^{-}_{peak} (kN)	α^{-}_{peak} (%)	P_{exp} (kN)	γ	γ'	θ_p (%)
S-NB	91.4	4.5	-98.9	-3.0	95.2	0.85	1.09	4.76
S-SC	92.1	3.75	-97.1	-3.0	94.6	0.85	1.08	4.89
S-MS	91.9	4.5	-101.4	-3.0	96.7	0.87	1.11	5.32
S-ES	93.8	4.5	-99.0	-3.0	96.4	0.86	1.10	5.41
Average					95.7	0.87	1.10	5.09
W-NB	76.2	3.0	-86.3	-3.0	81.3	0.80	1.05	3.90
W-SC	76.8	3.0	-83.4	-3.0	80.1	0.79	1.03	4.19
W-MS	76.3	3.0	-85.3	-3.0	80.8	0.79	1.04	3.94
W-ES	76.9	3.0	-84.8	-3.0	80.8	0.79	1.04	4.28
Average					80.7	0.80	1.04	4.08

Four D10 longitudinal steel bars, H 150×75×5×7 cross-sectional steel shapes, and transverse hoops made of D4 steel bars with 50 mm spacing were used. Both ends of the longitudinal steel bar and the H shape were connected to an end plate with welds. All the specimens are symmetrical with respect to their center lines. ASTM A36 steel was used for the H shape, and Grade 40 with a specified yield stress of 280 MPa was used for the steel bars. Mechanical properties of the steel used are listed in Table III.

There were 4 specimens in S series. In which, SBC connection, as shown in Fig. 6(a), was used. Considering the H steel shape only, the critical section is located 50 mm from the beam ends, as indicated in Fig. 7(a), with a moment capacity of M_p, where M_p is the plastic moment of H150×75×5×7 calculated with nominal yield stress of the steel. Projecting the moment capacity of the critical section to the beam end resulted in an equivalent beam end moment capacity, $(M_{cs})_{be}$, of $1.09M_p$.

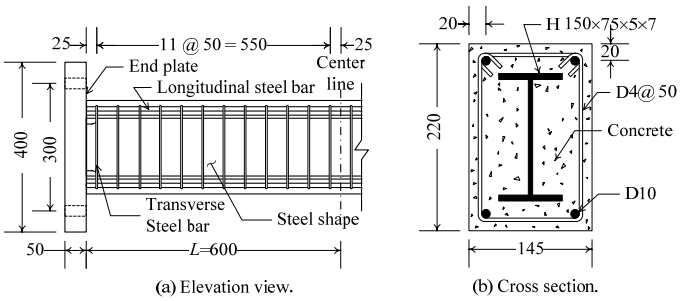

Fig. 5 Geometry and dimensions of specimens (unit: mm)

There were 4 specimens in W series. In which, WBC connection, as shown in Fig. 6(b), was used. Considering the H steel shape only, the moment capacity along the beam can be found in Fig. 7(b). The sections between C and D were designed to reach their moment capacity simultaneously, however, for the convenience of discussion, section C is designated as the critical section.

The moment capacity of the steel shape at section C was $0.85M_p$, which results in the $(M_{cs})_{be}$ of $0.93M_p$.

TABLE III
MECHANICAL PROPERTIES OF THE STEEL USED

Steel		Yield stress (MPa)	Ultimate stress (MPa)
H 150×75×5×7	Web	292	390
	Flange	272	376
D4		275	343
D10		331	491

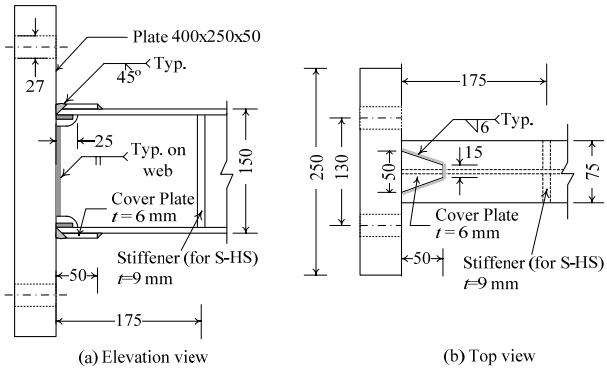

(a) SBC connection

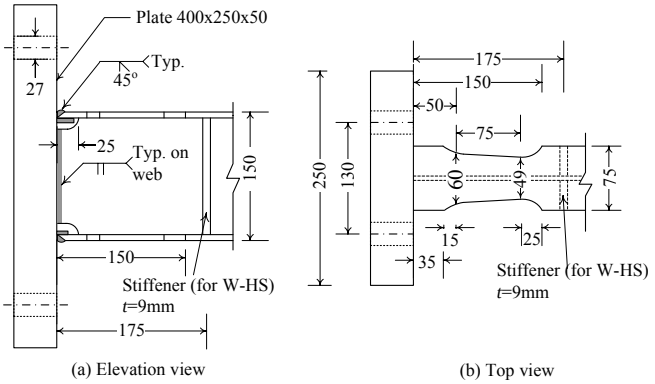

(b) WBC connection

Fig. 6 Detail of beam-to-column connection for the H shape (unit: mm)

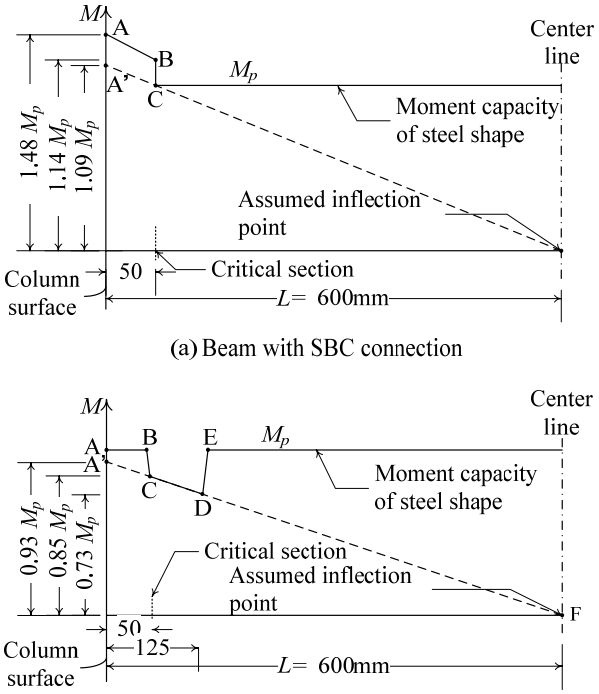

Fig. 7 Moment capacity distribution of the H shape

The specimens with 'SC' in their designation were equipped with shear connectors, as shown in Fig. 8(a). The specimens with 'MS' in their designations had a mid-span stiffener installed, as shown in Fig. 8(b). The specimens with 'HS' in their designations were had one mid-span stiffener and two plastic hinge zone stiffeners installed, at the position 175 mm from the end plate, as shown in Figs. 6 and 8(b). Specimens with 'NB' in their designations used neither shear connector nor stiffener, only natural bond was provided.

The average concrete compressive strength within the time span that the specimens were tested was 34.8 MPa.

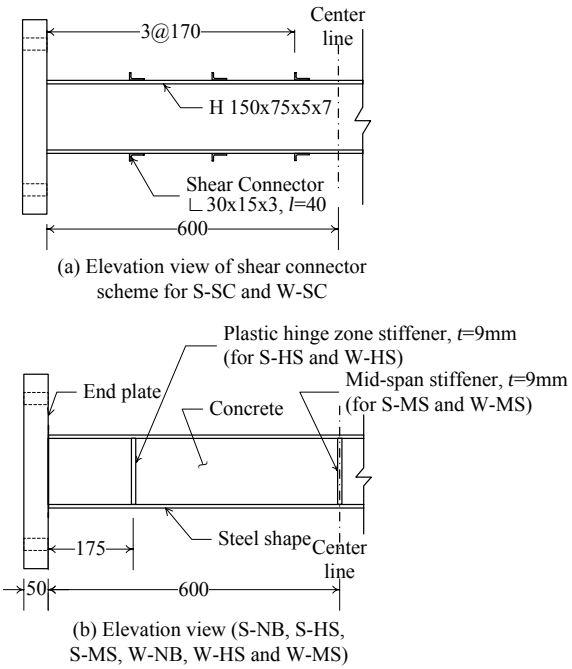

Fig. 8 Concrete constraint scheme

B. Test setup and loading procedure

The test setup is shown in Fig. 9. The bottom ends of the columns were connected through pin connections to a base beam that was tied down to the strong floor. A servo-controlled hydraulic actuator was connected to the right column. The actuator had a capacity of 500 kN and was equipped with a built-in load cell and built-in linear variable differential transducers (LVDT) to measure the force (P) and the lateral displacement (Δ) at the load point, which is defined as displacement of the right column. The displacement of the left column was also measured by an LVDT at the beam center. Rotation gauges R1 and R2 were installed on the end plates of the beam and rotation gauges R3 and R4 were installed 175 mm from each beam end.

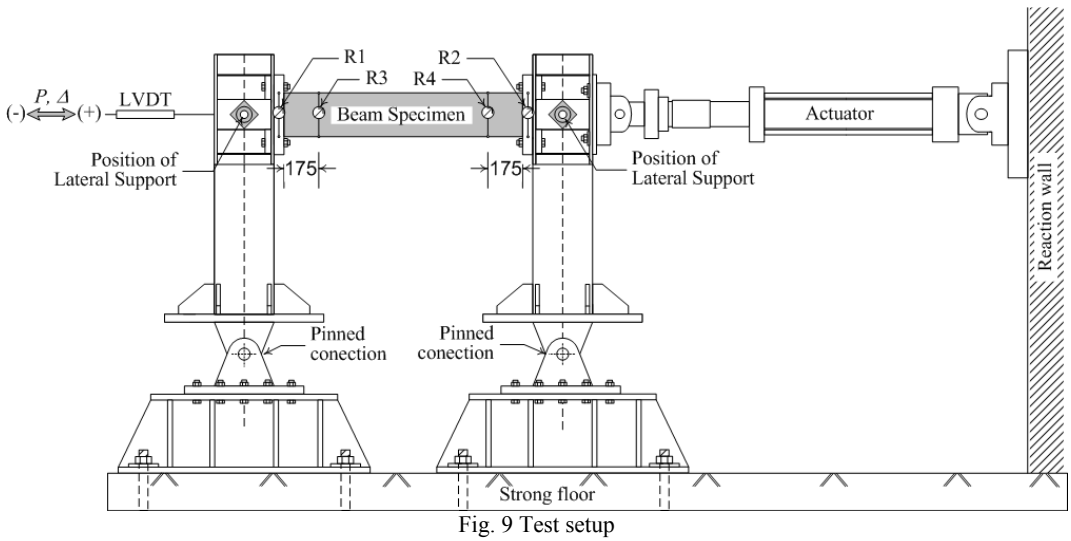

Fig. 9 Test setup

Loading was applied under displacement control according to the lateral displacement history shown in Fig. 10. Δ_y is defined as the lateral displacement of the frame when the nominal lateral strength P_n is applied. P_n is the loading under which the beam end moment, as indicated in Fig. 11, reached its nominal flexural strength (M_n). M_n was calculated using the actual material strength and the plastic stress distribution method as specified in AISC code [7]. According to the equilibrium condition of the frame shown in Fig. 11, P_n can be obtained by using (1).

$$P_n = \frac{0.5L_s}{0.5L_b} \cdot \frac{2M_n}{L_c} = \frac{8}{3}\frac{M_n}{L_c} \quad (1)$$

Δ_y of 9 mm was determined by using specimen S-NB, and used for all the specimens. The load test ended when the strength of the specimen deteriorated more than 20%.

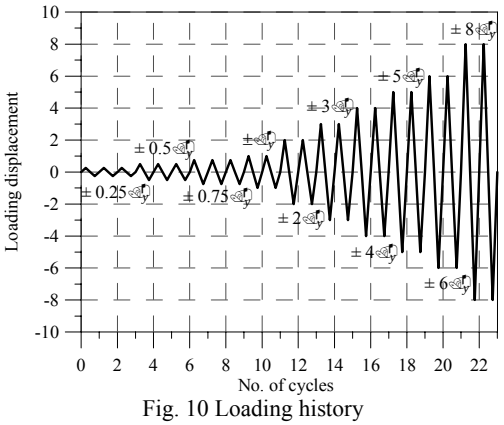

Fig. 10 Loading history

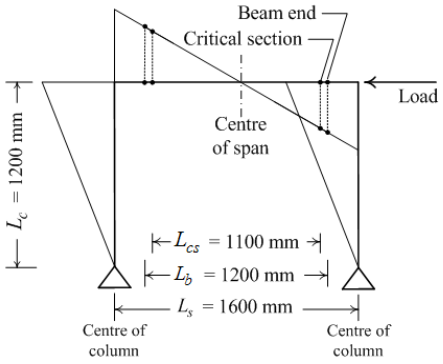

Fig. 11 Moment distribution of the frame

III. Experimental Result and Discussion

The load versus displacement hysteretic loops for the specimens are shown in Fig. 12 and the test results are summarized in Table II. The displacement of the frame is taken as the average of the right column displacement and the left column displacement. The maximum loads in the positive and negative directions are designated, respectively, as P^+_{peak} and P^-_{peak}. The drift angle of the frame is defined as the corresponding displacement divided by L_c.

The drift angles corresponding to P^+_{peak} and P^-_{peak} are designated as α^+_{peak} and α^-_{peak}, respectively. The maximum load for the tested specimen (P_{exp}) is defined as the average of P^+_{peak} and P^-_{peak}.

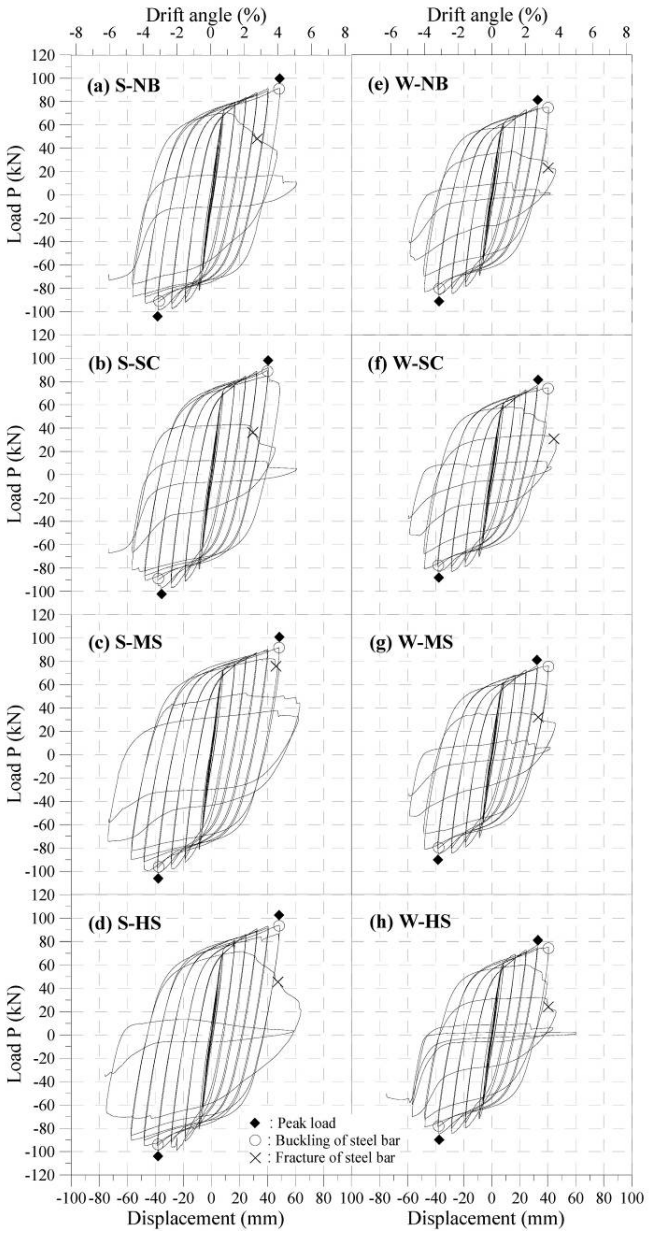

Fig. 12 Load versus displacement hysteresis loops

By assuming an anti-symmetrical moment distribution for the beam and applying the equilibrium of the frame shown in Fig. 11, the moment at the critical section corresponding to P_{exp}, designated as M_{exp}, can be calculated by using (2).

$$M_{exp} = \frac{1}{2}P_{exp}L_c\frac{0.5L_{cs}}{0.5L_s} = 0.344P_{exp}L_c \quad (2)$$

It is worth noting that $M_{\exp}$ is very likely to be an underestimate since the strength of the beam at both ends may not be developed at the same time. The calculated moment capacity at the critical section, designated as M_{na}, is calculated by using the actual material strength and plastic stress distribution method as specified in the AISC code [7]. The M_{na} for S and W specimens were respectively 46.09 and 42.01 kN-m. The strength ratio γ is defined as $M_{\exp}/M_{na}$.

The rotation of the left and right plastic hinge zones of the beam are designated as θ_L and θ_R, respectively. θ_L was calculated by subtracting R3 readings from R1 readings, and θ_R was calculated by subtracting R4 readings from R2 readings. Fig. 13 shows the lateral load versus plastic hinge rotation hysteresis loops for specimen S-HS. Fig. 14 shows positive P versus θ_L skeleton curve based on the first cycle of each drift angle excursion. The ultimate rotation θ^+_{uL} is defined as the rotation corresponding to 85% of P^+_{peak} in the descending portion. The elastic rotation θ^+_{yL}, as indicated in Fig. 14, is the estimated elastic rotation corresponding to P^+_{peak}. The plastic hinge rotation capacity θ^+_{pL} was the difference between θ^+_{uL} and θ^+_{yL}. Through the procedure aforementioned, θ^+_{pL}, θ^-_{pL}, θ^+_{pR}, and θ^-_{pR} for each specimen were determined. The plastic hinge rotation capacity, θ_p, of each specimen is defined as the average of θ^+_{pL}, θ^-_{pL}, θ^+_{pR}, and θ^-_{pR}.

More detailed observations of the cyclic behavior of the tested specimens are presented in the following sections.

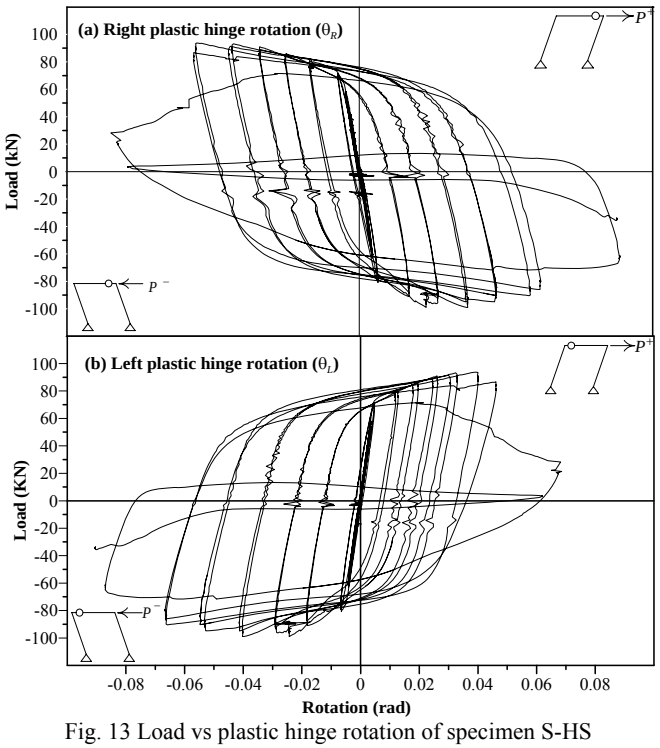

Fig. 13 Load vs plastic hinge rotation of specimen S-HS

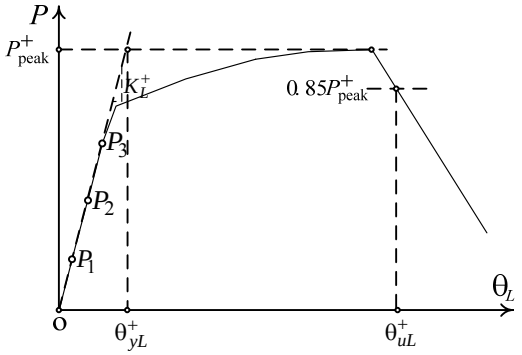

Fig. 14 The definition of θ_u and θ_y

A. S Series

During the loading tests, and the specimens were subjected to relatively high axial tension under positive load and axial compression under negative load. Compressive axial force resulted in higher beam moment capacity, while tensile axial force had an opposite effect. Therefore, P^-_{peak} is greater than P^+_{peak} for all specimens. The axial forces also caused the specimens to elongate significantly during the loading test. The axial elongation histories of all the specimens in the S series are very similar. Fig. 15(a) shows the axial elongation history of specimen S-NB.

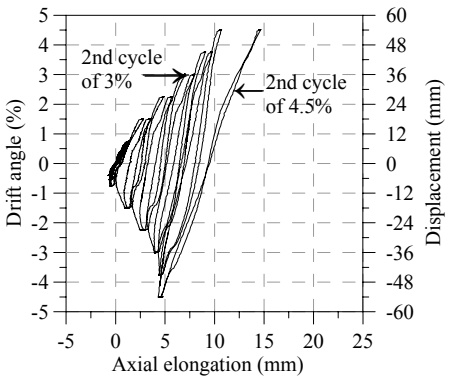

(a) Specimen S-NB

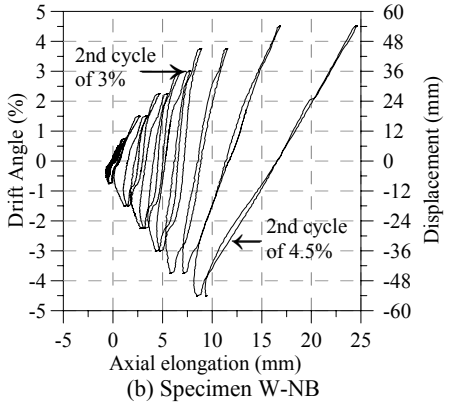

(b) Specimen W-NB

Fig. 15 Axial elongation history

The failure procedure was similar for all the specimens. Concrete crushing was followed by longitudinal steel bar

buckling and then fracture of the buckled steel bars when they were in tension. Fig. 16 shows the fracture of the steel bar of specimen S-SC. Compressive axial force made the specimen stiffer while tensile axial force reduced the specimen's stiffness. Consequently, the development of strength and failure of the specimens occurred faster, i.e. under a smaller drift ratio, when the load was in the negative direction. The crack pattern of the specimens after the 2nd 4.5% cycle is shown in Fig. 17(a~d). Since the buckling of the longitudinal steel bars played an important role in the failure process, the hoop spacing (S) to longitudinal steel bar diameter (d_b) ratio is an important parameter that affects the ductility of the encased type beams. The S/d_b ratio of the test specimens was 5. The limitation of S/d_b by ACI code is 8.

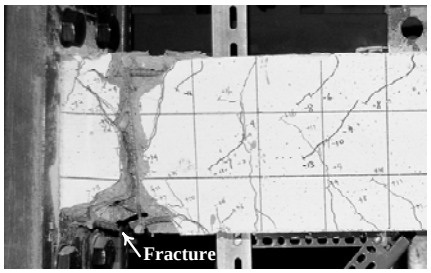

Fig. 16 Fracture of the steel bar of Specimen S-SC

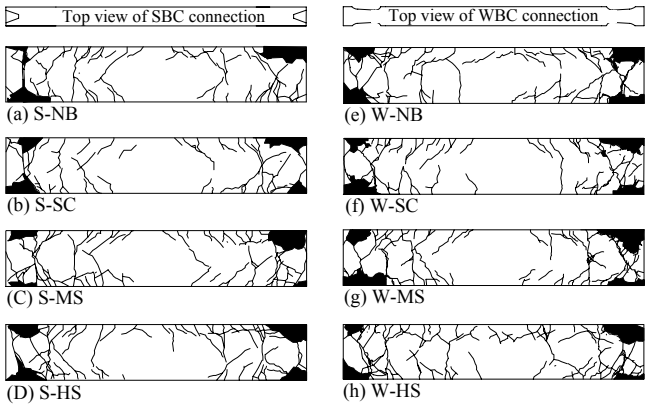

Fig. 17 Crack pattern for S and W series at 4.5% drift angle cycle

The $P_{\exp}$ value of specimens ranged from 94.6 to 96.7 kN, with an average value of 95.7 kN. The critical section is located 50 mm from the beam end; therefore, the $(M_{exp})_{cs}$ can be calculated according to (2). The γ ranges from 0.85 to 0.87 and is significantly less than one. Previous research [1], [8] shows that steel reinforced steel beams demonstrated significant composite action. Therefore, the lower $(M_{exp})_{cs}/(M_n)_{cs}$ should come from other factors, instead of lack the composite action. The significant axial elongation is considered to have caused most of the concrete to be ineffective in developing the beam's flexural strength. By totally neglecting the concrete part and using the plastic strain distribution method, the calculated moment capacity at the critical section, M_{nR}, is 36.07 kN-m.

The strength ratio γ', which is defined as $M_{\exp}/M_{nR}$, ranges from 1.08 to 1.11, which shows that the concrete still has some contribution to the flexural strength, especially when the specimen is loaded in the negative direction.

The θ_p ranged from 4.76 to 5.41% with an average value of 5.09 %. All S specimens showed sufficient plastic hinge rotation capacity for seismic design.

B. W Series

The W series specimens were also subjected to a relatively high axial force during the loading, therefore, P^-_{peak} was greater than P^+_{peak}, and the specimens elongated during the loading test. The axial elongation histories of all the specimens were very similar. Fig. 15(b) shows the elongation history of W-NB. Specimens W-NB and S-NB (Fig 15(a)) show similar elongation histories up to 3% drift angle, but specimen W-NB elongated more after that.

The failure procedure for all the specimens was similar to that of S series specimens. The tapering of the flange lead to a larger axial elongation and stress concentration, which caused extra damage to the concrete in the plastic hinge zone, as can be seen in Fig. 18. Consequently, the failure development of W specimens was faster than that of S specimens, and the cyclic performance of the W specimens is inferior to S specimens. The crack pattern of the specimens after the 2nd 4.5% cycle is shown in Fig. 17(e~h).

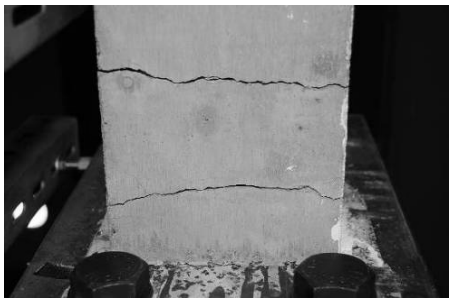
(a) Specimen S-NB

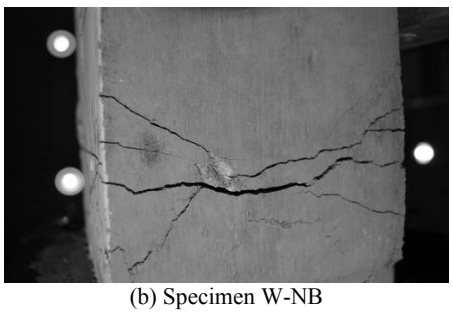
(b) Specimen W-NB
Fig. 18 Concrete cracks in bottom of the beam at 2.5% drift angle cycle

The $P_{\exp}$ value ranges from 80.1 to 81.3 kN with an average value of 80.7 kN. The M_{nR} of W specimens is 31.98 kN-m. The γ ranges from 0.79 to 0.80, and γ' from 1.03 to 1.05. This indicates that the concrete has essentially no contribution to the beam flexural strength of the W series specimens.

The θ_p ranged from 3.90 to 4.28% with an average value of 4.08 %.

C. The Effectiveness of Concrete Constraint Scheme

Take the specimen installed with shear connectors (SC specimen) in each series as a reference. The $P_{\exp}/(P_{\exp})_{SC}$ ratio and $\theta_p/(\theta_p)_{SC}$ ratio of specimens with NB, MS and HS are calculate and listed in Table IV. Where, $(P_{\exp})_{SC}$ and $(\theta_p)_{SC}$ are the $P_{\exp}$ and θ_p of the SC specimen in the same series.

TABLE IV
THE EFFECTIVENESS OF CONCRETE CONSTRAINT SCHEME

Concrete constrain	S series		W series	
	$P_{\exp}/(P_{\exp})_{SC}$	$\theta_p/(\theta_p)_{SC}$	$P_{\exp}/(P_{\exp})_{SC}$	$\theta_p/(\theta_p)_{SC}$
NB	1.01	0.97	1.01	0.93
MS	1.02	1.09	1.01	0.94
HS	1.02	1.11	1.01	1.02

The $P_{\exp}/(P_{\exp})_{SC}$ for all specimens ranged from 1.01 to 1.02. This is indicates that irrespective of the stress transfer types used, their contribution to the strength is roughly the same. Furthermore, the $P_{\exp}/(P_{\exp})_{SC}$ for NB specimens is 1.01. It shows that the constraint to the concrete provided by the column has a positive effect on the strength development of beam. From the values of $\theta_p/(\theta_p)_{SC}$, it shows that the intermediate stiffeners have obvious effects on enhancing ductility of the beams with SBC connection. The plastic hinge zone stiffeners in addition to mid-span stiffeners contribute better ductility than mid-span stiffeners installed alone. It indicates that the intermediate stiffeners, especially with plastic hinge zone stiffener installed, provide extra concrete confinement in the plastic hinge zone, which enhances the plastic hinge rotation capacity of the specimens. However, the stiffeners did not give extra ductility for specimens with WBC connection. That's because the flange tapering itself already resulted in uniform stress distribution of the flange in the tapering region, therefore, plastic hinge zone stiffeners can not bring extra ductility to the beam.

D. Strengthened and Weakened Steel Beam-to-Column Connection

Although the SBC and WBC are designed based on moment capacity of the steel shape instead of the whole section, the ductility behavior of all the specimens are quite satisfactory. It is much easier to design the beam-to-column connections based on steel shape alone instead of the whole section, and, test results from this study support this idea.

The average $P_{\exp}$ of S specimens (95.7 kN) is 19% higher than that of W specimens (80.7 kN). This phenomenon can be attributed to two factors. The first factor comes from the beam-to-column connection scheme itself. The equivalent beam end moment capacity $(M_{cs})_{be}$ for SBC is 1.09 M_p, which is 17 % higher than that of WBC (0.93 M_p). The influence of this factor reduces as the moment gradient of the beam becomes smaller. The second factor is the severer concrete damage to concrete near the flange tapering zone which inhibited the flexural strength development of specimens with WBC connection.

The θ_p of all the specimens is greater than 3%, which is considered sufficient for the structures in highly seismic zones. However, the average θ_p of S specimens (5.09%) is 25% higher than that of W specimens (4.08%). It may the concrete core within the plastic hinge length of W specimens does not effectively confined due to the severer concrete damage possessed by those specimens. The other possible reason is the RBS already provide plastic deformation enlargement so the additional treatment in order to improve the ductility behavior does not efficient.

REFERENCES

[1] Chen C.C. and Chen C.C., "Flexural behavior of steel encased composite beams," *Journal of the Chinese Institute of Civil and Hydraulic Engineering*, vol. 13, pp. 263-75, Feb. 2001.
[2] Plumier A., "Behavior of connections," *Journal of Constructional. Steel Research*, vol. 29, pp. 95-119, 1994
[3] Chen, S.J., Yeh, C.H. and Chu, J.M., "Ductile steel beam-to-column connection for seismic resistance," *Journal of Structural Engineering.-ASCE*, vol. 122, pp. 1292-9, Nov. 1996.
[4] Chen, S.J., Chu, J.M. and Chou, Z.L., 'Dynamic behavior of steel frames with beam flanges shaved around connection," *Journal of Constructional Steel Research*, vol. 42, pp. 49-70, Jan. 1997.
[5] Kim, T., Whittaker, A.S., Gilani, A.S.J., Bertero, V.V. and Takhirov, S.M., "Cover-plate and flange-plate steel moment-resisting connections," *Journal of Structural Engineering.-ASCE*, vol. 128, pp. 474-482, April 2002.
[6] Sumner, E.A. and Murray, T.M., "Behavior of extended end-plate moment connections subject to cyclic loading," J*ournal of structural engineering,-ASCE*, vol. 128, pp. 501-8, April 2002.
[7] AISC., Specification for structural steel buildings. American Institute of Steel Construction, 2005, Chicago. IL.
[8] Chen C.C. and Cheng C.L., "Flexural analysis and design methods for SRC beam sections with complete composite action. *Journal of the Chinese Institute of Civil and Hydraulic Engineering,* vol. 31, pp. 215-229, Feb. 2008.